Acta Cryst. (1977). A33, 445–455

Applications of Synchrotron Radiation to Protein Crystallography. II. Anomalous Scattering, Absolute Intensity and Polarization*†‡

BY JAMES C. PHILLIPS, ALEXANDER WLODAWER AND JULIA M. GOODFELLOW

Department of Chemistry and Stanford Radiation Project, Stanford University, Stanford, California 94305, *USA*

KEITH D. WATENPAUGH, LARRY C. SIEKER AND LYLE H. JENSEN

Department of Biological Structure, University of Washington, Seattle, Washington 98195, *USA*

AND KEITH O. HODGSON

Department of Chemistry and Stanford Radiation Project, Stanford University, Stanford, California 94305, *USA*

(*Received* 8 *October* 1976; *accepted* 8 *December* 1976)

The synchrotron X-ray beam produced by the SPEAR storage ring at the Stanford Linear Accelerator Center has been used as a tuneable and intense source for single-crystal-protein diffraction experiments. A measurement of the absolute intensity of a focused, monochromatized X-ray beam gave a value of 3×10^9 photons s^{-1} at a wavelength of 1·74 Å for typical machine operating conditions. A series of *hk*0 precession photographs were obtained from a crystal of the Fe-containing protein rubredoxin to investigate anomalous scattering effects and study their use in phase determination. Seven discrete wavelengths of radiation were used, some above and some below the Fe *K* absorption edge (1·743 Å = 7·111 keV). The rubredoxin diffraction data showed intensity changes due to f' varying with wavelength as well as from Bijvoet differences. The Fe site could be correctly located from difference Patterson and Fourier maps based either on f' or f''. The signal to noise ratio at the iron site was enhanced by calculating combined f' and f'' maps. The phases of the Bragg reflections were also obtained from three films collected at different wavelengths. When compared with the known phases for rubredoxin, the differences average to 60°, which indicates that some phasing information was available even from the relatively poor data and that this method will be potentially useful in future applications. A method for calculating the Lp factor which has to be applied to precession photographs taken with the polarized synchrotron X-ray beam is described in the Appendix.

Introduction

Over the past five years, synchrotron radiation, produced by the acceleration of electrons or other charged particles in synchrotrons or storage rings, has been used increasingly to study X-ray diffraction phenomena.§ The high intrinsic collimation and consequent high intensity of synchrotron radiation make it especially useful for low-angle X-ray diffraction studies. Such experiments have been carried out at the DESY synchrotron in West Germany (Rosenbaum, Holmes & Witz, 1971; Barrington Leigh, Holmes & Rosenbaum, 1972; Barrington Leigh & Rosenbaum, 1974; Goody, Holmes, Mannherz, Barrington Leigh & Rosenbaum, 1975), at the VEEP-3 storage ring in Novosibirsk, USSR (Mokulskaya, Mokulskii, Nikitin, Anashin, Kuplipanov, Lukashev & Skrinskii, 1974) and at the synchrotron NINA at Daresbury, UK (Haselgrove, 1976; Bordas, Munro & Glazer, 1976). A low-angle diffraction camera has also been installed at the electron–positron storage ring SPEAR at Stanford, USA (Webb, 1976; Webb, Samson, Stroud, Gamble & Baldeschwieler, 1976, 1977). We have previously reported (Phillips, Wlodawer, Yevitz & Hodgson, 1976) the use of this monochromator for single-crystal X-ray diffraction experiments with small protein crystals and also with a crystal having a large unit cell. A report comparing the intensity of conventional rotating anode sources with the DESY synchrotron for high-angle diffraction has been published by Harmsen, Leberman & Schulz (1976).

One of the important properties of synchrotron radiation for X-ray diffraction experiments is the availability of high intensity at wavelengths other than those associated with the characteristic emission lines of anode targets. Such characteristics make the synchrotron source uniquely suited to anomalous-diffraction experiments. For a diffraction experiment at a single wavelength, anomalous scattering from heavy

* Part I: Phillips, Wlodawer, Yevitz & Hodgson (1976).

† Partially supported by National Science Foundation Grant No. DMR 73-07692 in cooperation with the Stanford Linear Accelerator Center and US Energy Research and Development Administration.

‡ SSRP Report No. 76/09, October 1976.

§ The properties of synchrotron radiation and the research applications of this unconventional X-ray source have recently been reviewed in detail in *Synchrotron Radiation Research* (1976).

atoms is manifested in the Bijvoet differences. Blow (1958) and Blow & Rossmann (1961) proposed the use of these differences to assist in the phasing of protein diffraction data. Although multiple isomorphous replacement has been the basis of most structure determinations to date, a number of protein structures have been solved from only one isomorphous derivative plus anomalous differences. They include rubredoxin (Herriott, Sieker, Jensen & Lovenberg, 1970), ferrodoxin (Sieker, Adman & Jensen, 1972), flavodoxin (Watenpaugh, Sieker, Jensen, LeGall & Dubourdieu, 1972), phosphoglyceratekinase (Blake & Evans, 1974), hemerythrin (Stenkamp, Sieker, Jensen & Loehr, 1976) and penicillinase (Knox, Kelly, Moews & Murthy, 1976). Isomorphous derivative differences and Bijvoet differences can be combined to give improved Patterson maps for locating heavy atoms (Kartha & Parthasarathy, 1965). Matthews (1966) has shown how to scale these two types of differences and extended the method to difference Fourier techniques. Hoppe & Jakubowski (1975) were able to obtain phases for the protein erythrocruorin using two wavelengths available from X-ray tubes. Similar methods have been used in neutron diffraction experiments where neutrons of several wavelengths have been used in protein structure determination (Singh & Ramaseshan, 1968; Schoenborn, 1975). Raman (1959) and Herzenberg & Lau (1967) have also discussed such methods for use with X-ray diffraction data.

Such anomalous-dispersion techniques should be more easily accomplished with synchrotron radiation because the wavelength of the X-ray beam can easily be tuned around the wavelength of the K or L absorption edge for many heavy atoms. The real and imaginary components of the anomalous scattering can be selectively altered while other contributions to the diffraction pattern remain approximately the same. We have reported (Phillips *et al.*, 1976) preliminary results which indicate that an increase in the imaginary component could be detected for Fe by tuning to the K absorption edge, rather than with Cu $K\alpha$. In this report, we describe data from rubredoxin (an iron-containing protein) at seven wavelengths around the Fe K absorption edge. The data have been analyzed in terms of changes in the real (f')* and imaginary (f'') component of anomalous scattering with wavelength, and these changes, both separately and in combination, are used to obtain information about the location of the Fe atom and about the phases of the reflections.

Since synchrotron radiation is nearly totally polarized in the plane of the electron orbit, a modified polarization correction is essential. Such a modification, valid for precession films, is discussed in the Appendix.

* The nomenclature in this article follows the recommendation of the Proceedings of an Inter-Congress Conference on Anomalous Scattering (Ramaseshan & Abrahams, 1975) by expressing a scattering factor as $F = f + f' + if''$. However, $\Delta f'$ is used later in this paper to denote the change in f' from one wavelength to another.

Diffraction experiments

I. *Apparatus*

The experiments described were conducted at the Stanford Synchrotron Radiation Project, with radiation produced by the electron–positron storage ring SPEAR at the Stanford Linear Accelerator Center, Stanford, California. Winick (1974) has described in detail the characteristics of the synchrotron radiation from SPEAR. A typical operating cycle of the storage ring has also been described previously (Phillips *et al.*, 1976). Since that time some modifications have been made to the ring and the particle injection energy has been raised to 2·25 GeV, thus shortening the filling, energy ramping and orbit-adjusting procedure to about 30 min. When the experiments described here were being performed, the storage ring was operating at 3·6 GeV and the current during a fill was decaying exponentially from 30 to 15 mA giving a time-averaged current of approximately 20 mA over a period of approximately 2·5 h.

The polychromatic X-ray beam from the storage ring is focused and monochromatized by a Si[111] crystal/glass mirror monochromator (Webb *et al.*, 1976). The wavelength can be easily altered by changing the Bragg 2θ angle of the monochromator crystal, with a remotely controlled stepping motor. For small changes of wavelength, no refocusing of the beam is necessary.

In changing the wavelength of the monochromatized beam one also alters the angle at which it leaves the monochromating crystal. Therefore the apparatus used in the diffraction experiment must be realigned. An Enraf–Nonius precession camera with a pinhole collimator was used to record diffraction patterns. To align the camera with the X-ray beam, a base with two remotely controlled movements was constructed. The camera can be moved horizontally in a direction approximately perpendicular to the X-ray beam, and pivoted about a vertical axis passing through the middle of the collimator with remotely controlled stepping motors. By employing an ion chamber to monitor the intensity of the X-rays passing through the axis of the camera, one can deduce in which directions to move the camera to maximize this intensity, and thus align the camera. Initially, the height of the camera had to be adjusted manually, but it was then found that each time the incident wavelength was changed, the two motorized movements were sufficient to accurately realign the camera in a few minutes. To check the alignment, the shape of the beam after passing through the camera was recorded on Polaroid type 57 instant film. When the camera is properly aligned, one observed a perfectly circular spot.

II. *Intensity of the X-ray beam*

The intensity of the focused X-ray beam was obtained by measuring the fluorescence from an elemental Fe sample placed in the beam (Sparks, 1976). Direct

measurement of the intensity of the beam is difficult since, to bring the intensity down into the linear range of a good detector, the beam must be attenuated by a large factor. The beam from the synchrotron source also contains higher harmonics of the fundamental wavelength which are diffracted by the monochromating crystal. The mirror of the monochromator reflects these harmonics much less efficiently than it does the fundamental wavelength, but nevertheless the beam exiting the monochromator is reported to have a 0·1 % contribution to the intensity (photons s^{-1}) from the third harmonic (Webb, personal communication). This higher harmonic is attenuated much less rapidly than the fundamental wavelength. A numerical example will best illustrate this. If aluminum foil is used as an attenuator and the fundamental wavelength is close to the Fe K absorption edge, the fundamental wavelength will be attenuated by a factor of 1000 by a foil 0·36 mm thick, while the third harmonic will be attenuated by only 30 %. The attenuated beam would thus have a harmonic content of 41 %. Attenuating the first order by 10^6 halves the third order and the harmonic content would jump from 0·1 to 99·8 %. The results are similar if one assumes a fundamental wavelength close to Cu $K\alpha$. Thus the small harmonic content, which is insignificant for the purposes of diffraction experiments, makes any direct measurement of the beam unreliable.

The fluorescent intensity from a thick iron slab placed in the beam at an angle of 45° was measured using a photomultiplier tube placed perpendicular to the main beam and pointing towards the iron. The output of the photomultiplier tube passed in turn through an amplifier and a single-channel analyzer to a scaler. This setup enabled us to measure the fluorescent photon flux.

For a wavelength just above the Fe edge the fluorescent intensity was $1{\cdot}6 \times 10^5$ photons s^{-1} mm^{-2} of detector aperture. After corrections were made for the detector to iron sample distance and for absorption by air, the main beam intensity was calculated from the known cross-sections for capture of an X-ray photon by an Fe atom and the subsequent emission of a fluorescent photon as described by Sparks (1976).

The measured flux was 3×10^9 (± 20 %) photons s^{-1} in a focal spot of 0·5 × 0·5 mm at a wavelength of 1·74 Å. The storage ring was operating at 3·4 GeV and 14 mA. This measurement was made at a different time from the diffraction experiments reported in this paper. The best routinely obtainable operating conditions of SPEAR for the production of X-rays are 3·7 GeV and 45 mA and under these conditions, the intensity would then be about 10^{10} photons s^{-1}. In the diffraction experiments reported here a pinhole collimator was used to define the beam. This reduces the intensity available for experiments, but the estimates of the beam intensity from the exposure times of diffraction patterns recorded on film indicated that this loss is not substantial (Phillips *et al.*, 1976).

The intensity of a focused, monochromatized X-ray beam from the synchrotron DESY has been reported by Harmsen, Leberman & Schulz (1976). The measured flux was considerably lower than that from the monochromator at SPEAR, as is expected on the basis of machine parameters. The intensity expected from the storage ring DORIS is about the same as for SPEAR. Table 1 lists the results of both the SPEAR and DESY measurements and their comparisons with conventional sources (as measured by Harmsen *et al.*, 1976). It should be noted that the natural collimation of the synchrotron beam makes the intensity gain relatively larger for crystals with large unit cells and for low-angle diffraction.

As we reported previously (Phillips *et al.*, 1976), the intensity of the synchrotron beam is considerably higher than for the $G \times 6$ rotating-anode generator even in the instances when high collimation of the beam is not required. The brightness of the beam will increase by an order of magnitude upon completion of a new 'diffraction' beam line, while the spectral bandwidth will be narrower (see Table 1).

III. *The choice of crystal*

Rubredoxin was chosen as a test protein for the

Table 1. *Intensity comparisons for conventional and synchrotron X-ray sources*

		DESY*	SPEAR 3·4 GeV 15 mA		
	G × 6* 1·6 kW	6·5 GeV 3·1 mA	'EXAFS' beam line	'Biology' beam line	'Diffraction' beam line
Monochromator	Ni filter	mirror-quartz	Si[220] channel cut (unfocused)	Si[111] mirror	Ge[220] channel-cut mirror
Beam size (mm)	0·2 × 0·2	0·2 × 0·2	1 × 20	0·5 × 0·5	1·6 × 3·5
$\Delta E/E$	20/8000		1/8000	30/8000	4/8000
Flux ($h\nu$ s^{-1})	$6{\cdot}4 \times 10^7$	2×10^7	1×10^{10}	3×10^9	$6{\cdot}7 \times 10^{11}$‡
Brightness ($h\nu$ mm^{-2} s^{-1})	$1{\cdot}6 \times 10^9$	5×10^8	5×10^8	$1{\cdot}2 \times 10^{10}$	$1{\cdot}2 \times 10^{11}$‡
Relative brightness	1†	0·32	0·32	7·5†	75‡

* Harmsen *et al.* (1976).
† Phillips *et al.* (1976). Observed difference in exposure times for this configuration is over sixfold.
‡ Predicted.

crystallographic studies described herein for several reasons. Rubredoxin is a protein of molecular weight 6000 and contains one Fe atom per molecule. It crystallizes with one molecule per asymmetric unit. It should thus be possible to detect the anomalous scattering from the Fe in the diffraction pattern. The crystal structure has been solved and refined at a resolution of 1·5 Å (Watenpaugh, Sieker, Herriott & Jensen, 1973). The Fe atom position and the phases of the Bragg reflections are known with high precision. The crystals are relatively stable in the X-ray beam and the diffraction pattern has been observed to 1·2 Å resolution.

Rubredoxin crystallizes in the space group $R3$. The $hk0$ reciprocal lattice plane is non-centrosymmetric and thus one can calculate projection Patterson and Fourier maps using Bijvoet differences as the amplitudes of the coefficients to locate the Fe site. A precession photograph of the $hk0$ zone contains all the intensity data necessary to calculate a projection map. Therefore, in an investigation of the effect that changing wavelength has on the contribution of anomalous scattering to the diffraction pattern, one photograph per wavelength is sufficient.

IV. *Measurements*

Seven 25° precession photographs of the $hk0$ reciprocal-lattice plane of rubredoxin were collected (Fig. 1). Exposure times varied from 5 to 6 h. The same $0{\cdot}6 \times 0{\cdot}6 \times 0{\cdot}3$ mm crystal was used for all the photographs and was previously exposed for a considerable length of time to X-rays from a conventional tube. There was little fall-off of diffracted intensities during the course of data collection. The X-ray beam wavelength was altered for each exposure. Wavelengths on both sides of the K edge of Fe (1·743 Å = 7·111 keV) were used. The detailed shape of the absorption edge of Fe has not been studied, but the recently reported studies of edge shape of Ga should be applicable. Fig. 2 shows the variation of f' and f'' for Ga close to the Ga K absorption edge (after Fukamachi & Hosoya, 1975). The wavelength (λ) is given in the reduced reciprocal units of λ_e/λ where λ_e is the K edge wavelength for Ga (1·19 Å = 10·4 keV). Also marked are the wavelengths at which rubredoxin diffraction data were collected. They are given in units of λ_e/λ where λ_e is now the Fe K edge wavelength. Fig. 2 is schematic; the detailed structure of the Fe edge is unknown but it is generally thought that the gross features of K absorption edges are similar.

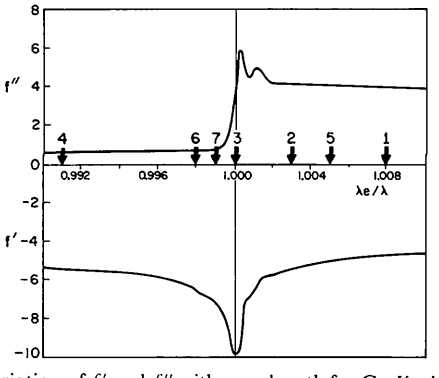

Fig. 2. Variation of f' and f'' with wavelength for Ga K edge. Wavelengths are in the units of λ_e/λ where λ_e is the wavelength of the absorption edge. Similar curves are expected for Fe. The arrows indicate relative wavelengths at which data were recorded.

To find the correct monochromator settings for wavelengths close to the Fe edge, the transmission of an Fe foil as a function of the settings was measured. An increase in the transmission indicated that the K edge had been exceeded. Wavelengths were measured by taking precession photographs of a crystal of $SrAlF_6$ and comparing them with one taken with Cu radiation (the spots produced by the $K\beta$ line being taken as standard). This method should be accurate to 0·07% (Patterson & Love, 1970).

The rubredoxin films were densitometered with a computer-controlled Optronics rotating-drum film scanner (Matthews, Klopfenstein & Colman, 1972) at the University of Oregon.

Data analysis

I. *Bijvoet differences as a function of wavelength*

The $hk0$ reciprocal-lattice plane of a crystal in the space group $R3$ possesses threefold symmetry. There is pseudo sixfold symmetry, broken only by Friedel-pair splitting. All six symmetrically related diffraction spots are present in the diffraction patterns from rubredoxin (Fig. 1). The average deviation from the mean (D) for each film was calculated with the standard formula $D = \sum|I - \bar{I}|/\sum I$, where I and $\bar{I}$ are respectively the intensity of a reflection and the average intensity of symmetry-related reflections. The results of calculating average D values for the precession photographs first assuming threefold (D_3) then sixfold (D_6) symmetry are shown in Table 2. The ratio $D_{63} = D_6/D_3$ is an approximate measure of the contribution of the imaginary part of the anomalous scattering (f'') to the diffracted intensities. The figures for films 1, 2, 4, 5 and 6 show that f'' is considerably greater above the edge (in energy) than it is below. The intermediate values for films 3 and 7 indicate that the bandwidth of the monochromatized radiation is wider than the absorption edge. The beam incident on the crystal is thus a mixture of 'above-edge' and 'below-edge' components for these two films. Webb (1976) gives a value of 10^{-2} Å for the bandpass of the monochromator at 1·74 Å. The actual values of D_3 and D_6 vary considerably, indicating that we are comparing data sets of different quality. Also, radiation damage to the crystal is increasing somewhat from one film to the next (the exposures being numbered in the order in which they were taken). However, D_{63} does not appear to be a function of D_6, D_3 or the radiation dose alone. It should be noted that D_6 will

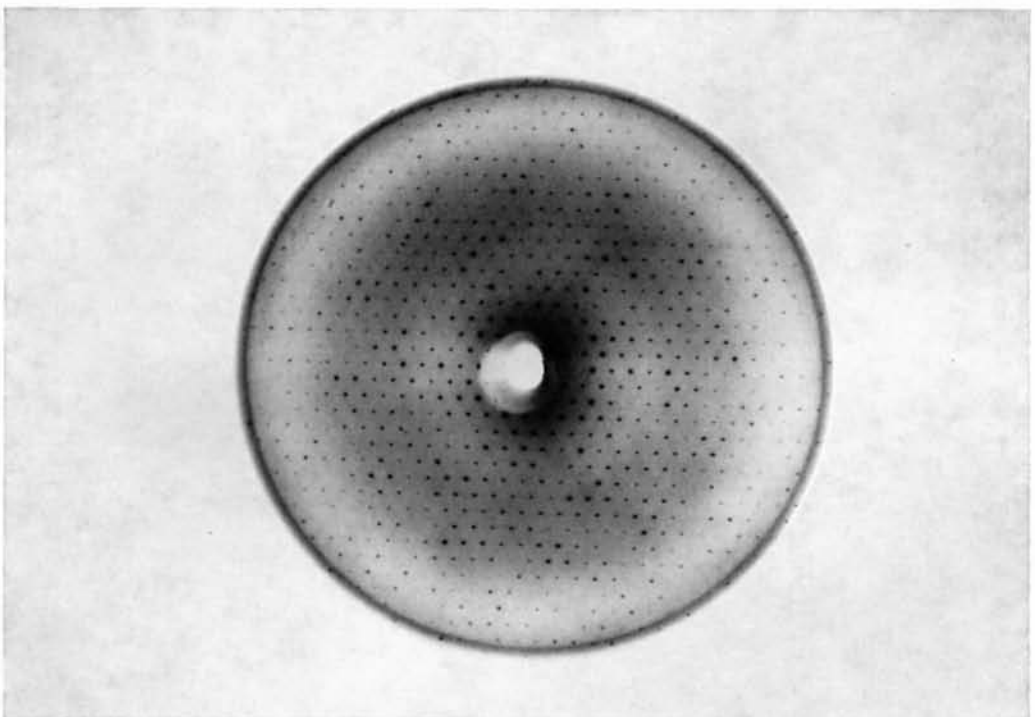

Fig. 1. *hk*0 precession photograph (No. 4) of rubredoxin recorded with synchroton radiation at $\lambda = 1.758$ Å, $\mu = 25°$ with an exposure time of 5.5 h.

[*To face p.* 448

be greater than D_3 simply because more values are being averaged. Thus the values of D_{63} for films 4 and 6 do not necessarily indicate that there is Bijvoet-pair splitting at these wavelengths.

Cross-correlation coefficients, C_{ij}, were calculated for all 21 possible pairings of the seven films where $C_{ij}=\sum_{\mathbf{h}} \Delta_i\Delta_j/[(\sum_{\mathbf{h}} \Delta_i^2)(\sum_{\mathbf{h}} \Delta_j^2)]^{1/2}$ and Δ_i and Δ_j are the Bijvoet differences (with sign) as observed on the ith and jth film respectively with the summations extending over all reflections common to both films (Colman, Jansonius & Matthews, 1972). As an example, all values of C_{i1} are given in Table 2. The values of C_{ij} are always larger for pairs of films taken above the absorption edge in energy and decrease if one of the films was taken on or below the absorption edge.

II. *Patterson and Fourier maps based on f″*

Both Patterson and difference Fourier maps were calculated, in projection, for the data from all seven wavelengths using a program supplied by G. Reeke. The coefficients $(F_{hk0}-F_{\overline{hk}0})^2$ and $(F_{hk0}-F_{\overline{hk}0})\exp[-i(\varphi_{hk0}-\pi/2)]$, where φ_{hk0} is the phase of the $hk0$ reflection, were used for Patterson and difference Fourier maps respectively. The difference Fourier coeffficents were introduced by Kraut, High & Sieker (1964). The phases were those obtained from a refinement of a model of rubredoxin at 1·5 Å resolution (Watenpaugh *et al.*, 1973). All the maps were calculated on a 1 Å grid.

In an *ab initio* determination of the Fe atom position one would assume that the largest positive peak on the difference Patterson map (excluding the origin peak) was due to the Fe–Fe vector (remembering that there is only one Fe atom per asymmetric unit and therefore only one Fe–Fe atom vector in the space group $R3$). As a measure of the quality of the maps, the ratio Q was calculated for each map and defined as the ratio of the heights of the peak at the expected position for the Fe–Fe vector (or Fe site on a difference Fourier map) and the highest positive peak not at this position. The results are shown in Table 2. The largest feature on two out of three Patterson maps calculated from data taken above the absorption edge is found at the position expected for the Fe–Fe vector. However, the ratio Q decreases for longer wavelengths indicating that the Fe–Fe vector peak is becoming less prominent. Eventually at $\lambda=1{\cdot}746$ and 1·758 Å there is no trace of a peak at the correct position. The Patterson maps for the wavelengths 1·735 Å and 1·758 Å (films 5 and 4) are shown in Fig. 3(*a*) and (*b*). The contours are drawn at equal arbitrary levels and the lowest three contours are omitted. The expected position of the Fe–Fe vector is marked with a cross.

Similarly the largest feature on the difference Fourier maps is at the position expected for the Fe site but this peak is more prominent (*i.e.* Q has a higher value) on maps calculated from data collected above the absorption edge.

III. *Patterson and Fourier maps based on changes of f′ with wavelength*

As some data sets had been collected at wavelengths greater than λ_e for Fe, there was the possibility of observing intensity differences due to the dependence of f' on wavelength (with f'' remaining small and constant). The following theory has been developed in order to analyze the data in this manner. Fig. 4 shows the contributions to a diffracted wave from various parts of the protein molecule as vectors on the complex plane. OA is that from the protein. AB corresponds to the normal scattering from the heavy atom. BJ, BC and BF are the f' contributions at various wavelengths and JK, CD and FG are the corresponding f'' vectors. Depending on the wavelength of the incident radiation, one measures the amplitude OG, OD or OK for the hkl reflection. OD, OG and OK are measured with incident beam wavelength shorter than the absorption edge, about the same as the edge and slightly longer than the edge respectively. OH, OE and OL are the $\bar{h}\bar{k}\bar{l}$ reflections inverted through the real axis. The magnitudes of OA and AB relative to the anomalous scattering contributions have been grossly reduced for clarity. If the drawing were to be made to scale, OA would be the largest vector by far, for most reflections. AB is 5 to 10 times larger than f'' or f' at a K edge.

Table 2. *Summary of film statistics, cross-correlation and the quality of calculated maps*

For definitions, see text.

Film	λ ±0·002	λ_e/λ ±0·001	D_3 %	D_6 %	D_{63}	C_{i1}	Patterson Q	Patterson Comments	Fourier Q	Fourier Comments
1	1·730	1·008	8·3	10·0	1·21	–	0·99	One large noise peak	2·14	
5	1·735	1·005	6·4	8·2	1·29	0·71	1·90		2·57	
2	1·738	1·003	5·8	7·4	1·27	0·63	1·55		2·23	
3	1·743	1·000	6·7	8·0	1·18	0·26	0·96	Peak shifted	1·43	
7	1·744	0·999	7·3	8·2	1·12	0·48	0·75		1·11	
6	1·746	0·998	7·9	8·6	1·08	−0·03	0·38		1·27	Peak shifted
4	1·758	0·991	11·0	11·6	1·05	0·02	0·53		1·40	Peak shifted
Real part, films 7, 4							1·37		1·73	
Real part, films 6, 4							0·82		1·58	Peak shifted
Combined, films 1, 7, 4							1·57		2·71	
Combined, films 1, 6, 4							1·83		2·20	
Combined, films 2, 7, 4							1·59		2·50	
Combined, films 5, 7, 4							2·43		3·02	

Therefore, averaging Friedel pairs gives good approximations to OF, OC and OJ. Thus a Patterson map with $(OJ-OF)^2$ as coefficients is analogous to an isomorphous derivative Patterson map. Similarly, the difference Fourier coefficients $(OJ-OF)\exp(-i\varphi_{hk0})$ are analogous to those for an isomorphous derivative.

A Patterson map and a Fourier map were calculated with data from wavelength 1·744 Å (film 7) and data from 1·758 Å (film 4). Friedel pairs were averaged in each data set and the two data sets were scaled together. The Patterson and Fourier coefficients used were $(F_4-F_7)^2$ and $(F_4-F_7)\exp(-i\varphi_{hk0})$ respectively.

From the values of Q (Table 2) it can be seen that the largest peak on the map is at the position expected for the Fe–Fe vector on the Patterson (Fig. 3*c*) and at the expected Fe site on the difference Fourier map. In principle, data sets from any two wavelengths at which f' differs can be used in the above manner to locate the Fe atom. The results of attempts for another pair of films are given in Table 2. In general, all pairs of data gave results similar to those for below-the-edge Bijvoet pair maps.

To test whether the maps for films 4 and 7 were actually measuring a change in the real part of the anomalous scattering and not a mixture of the real and imaginary parts, a difference Fourier map was calculated with coefficients $(F_4-F_7)\exp[-i(\varphi-\pi/2)]$. As a control, a Bijvoet pair map for film 2 was calculated with coefficients $(F_{hk0}-F_{\overline{hk}0})\exp(-i\varphi)$. Neither of the wrongly calculated maps had any features greater than the noise peaks on the correct maps, thus it appears that f'' is not biasing the maps based on the real part of anomalous scattering.

IV. *Combined maps from f'' and f' differences*

It is possible to combine differences in f'' and f' with wavelength in an analogous manner to that used for combining Bijvoet and isomorphous derivative difference. Assuming f' and f'' are small compared with the scattering from the protein, OA, OF, OJ, OD and OE in Fig. 4 can all be considered parallel. Hence $OJ-OF=\Delta f'\cos\beta$ and $OD-OE=2f''\sin\beta$ where $\Delta f'$ is the change in f' from one wavelength to another. Analogous equations have been derived by Kartha & Parthasarathy (1965). Matthews (1966) showed how to determine the ratio k, where $k=(f+f')/f''$ (in our notation). A procedure similar to that of Matthews (1966) was used to determine the ratio $k'=\Delta f'/f''$.

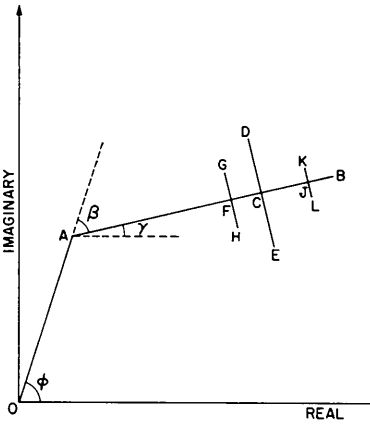

Fig. 4. Scattering vectors associated with the anomalous scattering at various wavelengths. Total scattering vectors are omitted for clarity. For details see text.

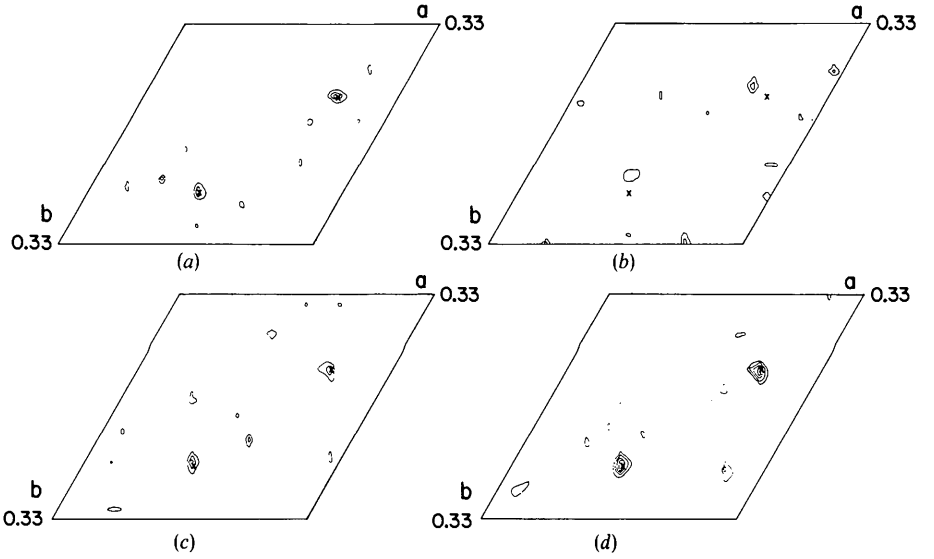

Fig. 3. Patterson maps of rubredoxin. Contoured on an arbitrary scale, the negative and three lowest positive contours omitted. Origin peak removed. (*a*) Bijvoet difference map. $\lambda=1{\cdot}735$ Å (film 5), above K edge of Fe in energy. (*b*) Bijvoet difference map. $\lambda=1{\cdot}758$ Å (film 4), below K edge in energy. (*c*) Difference Patterson map based on the changes in the real component of anomalous scattering. $\lambda=1{\cdot}744$ and 1·758 Å (films 7 and 4 respectively). (*d*) Patterson map with combined real and imaginary components. f' was calculated as in (*c*), and f'' as in (*a*).

Combined Patterson maps (*i.e.* with changes both in f' and f'') were calculated from

$$f''^2=(2/k')^2(F_4-F_7)^2+(F_{hk0}-F_{\overline{h}\overline{k}0})^2 \quad (1)$$

with $(F_{hk0}-F_{\overline{h}\overline{k}0})^2$ being Bijvoet pairs taken from films 1, 5 and 2 in turn. The map with f'' data from film 5 is shown in Fig. 3(*d*).

Difference Fourier coefficients were calculated by combining f'' and f' differences in an analogous manner to that used by Matthews (1966). Some simplifications are possible in our case. The value of β can be found from the equations above. With the known protein phase, φ, one can calculate the phase of the heavy-atom contribution from the equation

$$\varphi=\beta+\gamma \quad (2)$$

(Fig. 4). Thus, Fourier coefficients

$$f''\exp(-i\gamma)=\left[\left(\frac{2}{k'}\right)^2(F_4-F_7)^2+(F_{hk0}-F_{\overline{h}\overline{k}0})^2\right]^{1/2}\times\exp[-i(\varphi-\beta)] \quad (3)$$

were calculated. It should be noted that as the Fe in rubredoxin is naturally occurring, the protein phase angle corresponds to the angle between *OC* and the real axis in Fig. 4. This makes no difference to the argument within the approximations used.

The weighting of the real-part data with the anomalous data is not obvious as Q for the real-part maps is smaller than that for the f'' maps but the ratio k' indicated that $\Delta f'$ is larger than f'' in all maps for which this calculation was done. Therefore, no weighting factor was applied.

The values of Q for the combined Patterson and Fourier maps are given in Table 2. An improvement over the respective real-part and Bijvoet difference maps is noticeable.

'Combined' Patterson and Fourier maps were calculated with the worst set of above-edge Bijvoet differences ($\lambda=1{\cdot}730$ Å, film 1) and the second-best $\Delta f'$ data ($\lambda=1{\cdot}746$, $1{\cdot}758$ Å; films 6 and 4). The result (see Table 2) for the Patterson map shows that from two complementary, but by themselves inadequate, data sets a correct map can be calculated.

V. *Phase determination*

The phase γ of the heavy-atom contribution was calculated from the positions of the heavy atoms as derived from the Patterson maps. From equation (2), an estimate of the protein phase, φ, was obtained. These phases for the *hk*0 reflections of rubredoxin differed by approximately 60° (on average) from the phases of the refined model of Watenpaugh *et al.* (1973). This should be compared with a 90° difference for random phases and 35° difference between the initial multiple isomorphous replacement and final refined phases of these *hk*0 reflections found by Watenpaugh *et al.* (1973).

Discussion

The intensities of X-ray beams expected from synchrotron radiation facilities have been a subject of considerable disagreement, since they are difficult to calculate theoretically and depend strongly on the monochromator, required collimation, focal-spot size, and the distance between the camera and the source. Our measurement of 3×10^9 photons s^{-1} at the focal spot of the 'biology' beam line at SSRP is much higher than that reported by Harmsen *et al.* (1976) for the synchrotron DESY, as could be expected by comparing the parameters of the two machines. In general, the intensity from storage rings exceeds that from the synchrotrons, because of higher currents and better beam stability. At present, the intensity from SPEAR for high-angle diffraction is 6–7 times better than from a conventional 1·6 kW rotating anode source, and another improvement of an order of magnitude should be accomplished when the new 'diffraction' beam line is completed.

The anomalous components of scattering by Fe could be detected, even though actual phasing of reflections was made difficult by poor-quality data as indicated by D values in the range 5·8–11 %. Both the values of D_{63} and C_{i1} correlate very well with the wavelength of incident radiation (Table 2), being much higher above the absorption edge and lower below. Intermediate values just next to the edge are due to the excessive bandwidth of radiation used. Correlation coefficients for other films behave in a similar manner. All Patterson maps calculated from anomalous data with $\lambda<\lambda_e$ have a large peak at the expected position of the Fe–Fe vector as seen from the values of the ratio Q, in Table 2, while those from data with $\lambda>\lambda_e$ do not. This is to be expected and confirms that the change of the anomalous scattering with wavelength can be detected.

It has long been recognized that a change of f' with wavelength affects the diffraction pattern in the same way as does the insertion of a heavy atom in the structure (Raman, 1959; Ramaseshan, 1964). To the authors' knowledge, only one X-ray diffraction study of a protein structure has used multiple-wavelength techniques to obtain phases (Hoppe & Jakubowski, 1975). Two wavelengths were used to study the protein erythrocruorin. One was shorter than the absorption edge of the heavy atom in the structure (also Fe), and one was longer. The wavelengths were 1·659 Å (Ni $K\alpha$) and 1·790 Å (Co $K\alpha$). Separate Patterson maps were calculated with the coefficients (in the notation of Fig. 2) $(OD-OG)^2$ and $(OE-OH)^2$, but no 'combined' maps were presented.

While the ratio Q for a map calculated with the real part of anomalous scattering was lower than for Bijvoet differences, the position of the Fe atom could be located if the two wavelengths were appropriately chosen. It thus seems that to measure best the change in f' with wavelength one should make measurements close to and far from the K edge, but always below, in energy.

This is in accord with the variation of f' with wavelength reported by Fukamachi & Hosoya (1975).

Matthews (1966) has discussed how to weight the isomorphous and Bijvoet difference data and how to get a better approximation to 'exact' Patterson and Fourier coefficients by calculating the angle between the protein and the protein plus heavy-atom vectors. In our case, the real-part maps are worse than the f'' maps but the ratio k' indicates that $\Delta f'$ is larger than f'' in all the maps calculated. It was therefore not obvious how to weight the data and no such weighting was used. In retrospect, it appears that the Bijvoet differences were observed more reliably, since there were no errors resulting from scaling of different films.

Also the geometry of the addition of the vectors in the complex plane is not quite the same and one cannot correct for errors in the assumption that OA, OF and OJ are parallel. If one took data at 'matching wavelengths' such that points C and J in Fig. 4 coincided, *i.e.* such that the below-edge and above-edge values of f' were the same, then angle FOJ could be calculated and the result used to make such a correction. Since our knowledge of the fine structure of the K edge of Fe is incomplete, it is safest to assume that we do not have data from such 'matching wavelengths.' However, the errors involved in omitting this correction are not as large as if one were dealing with isomorphous replacement and Bijvoet difference data, as $\Delta f'$ is much smaller than the scattering of a heavy atom.

Matthews (1966) also noted that his parameter k is dependent upon $\sin\theta/\lambda$, primarily because the scattering factors of atoms of large radius fall off at high scattering angles. Since f' and f'' are both facets of the same phenomenon, it seems reasonable that they depend in the same way on $\sin\theta/\lambda$, and $\Delta f'/f''$ was assumed to be a constant for all reflections. A calculation revealed that k' increased slightly at higher values of $\sin\theta/\lambda$ but there are not enough reflections on the $hk0$ plane for this to be an accurate test.

These results confirm that a change in the real part of the anomalous scattering has been detected, that such a change is equivalent to obtaining an isomorphous derivative and that it can provide information useful in finding the heavy atom.

The results of this experiment suggest several ways in which a tuneable X-ray source can be used in the determination of a protein structure. Heavy atoms can be located on projection Patterson and Fourier maps based on changes in f' with wavelength. The data for a projection map can be collected much more rapidly than that for a three-dimensional map, an important practical consideration because experimental time at a synchrotron radiation source is usually limited. Real-part projection maps can be used to locate heavy atoms which are present in the native protein. If a Bijvoet difference map failed to locate a native heavy atom, a 'combined' map could be calculated. If the heavy atoms in a derivative cannot be found because of a lack of isomorphism with the native crystals, real-part or combined maps could be calculated. Such a derivative could be used for a multiple wavelength phase determination if no other derivatives were found.

Real-part maps depend on a large change in f' with a small change of wavelength. This occurs at an absorption edge. The absorption edges of different elements occur at different wavelengths, thus a real-part map will specifically locate one element. This could be useful if a crystal contained more than one kind of heavy atom and the resulting Patterson map could not be solved.

Hoppe & Jakubowski (1975) have shown how to measure a reflection and its Bijvoet pair at two wavelengths with sufficient accuracy to obtain a useful estimate of the phase. A diffractometer was used for data collection. The limit of the method is data-collection time. It was noted that a synchrotron radiation source would be ideal for such an experiment, especially for the possibility of selecting any wavelength of radiation, within the region of interest to crystallographers. The intensity available at SPEAR will enable reductions in the data collection time by a large factor. It has previously been estimated that the focusing monochromator at SPEAR has a flux 60 times greater than a 1·2 kW Cu $K\alpha$ sealed-tube X-ray source (Phillips *et al.*, 1976). Hoppe & Jakubowski (1975) used Ni $K\alpha$ and Co $K\alpha$ X-ray tubes operated at 420 W. One could expect that these sources provided less than 1 % of the intensity reported in this paper. At SPEAR, with the data-collection techniques of Hoppe & Jakubowski (1975), one could expect to obtain accurate phases in a far shorter time.

Hoppe & Jakubowski (1975) reported that the average difference was approximately 60° between the phases calculated on the basis of anomalous scattering and by multiple isomorphous replacement. There was an expected deviation of about 50° from the 'true' phases. The average deviation of the rubredoxin phase calculated on the basis of our data, as compared with refined phases of Watenpaugh *et al.* (1973), was 60°, even though the data-collection procedure was simpler than in the former study. Argos & Mathews (1973) achieved considerable success in calculating parts of the electron density map of cyctochrome b_5 based on the anomalous scattering of Fe, with an average phase discrepancy of about 55°, compared with MIR phases, indicating that the phase determination in the present study is useful. To combine the phase determination methods of Hoppe & Jakubowski (1975) with the unique features of synchrotron radiation, a four-circle goniometer is being installed at the Stanford Synchrotron Radiation Project.

Conclusion

We have measured changes in the diffraction pattern from a protein crystal, these changes being induced by tuning the incident X-ray wavelength across an absorption edge of a heavy atom in the protein. Such changes can be measured with sufficient accuracy to locate the

heavy atom, with film used as a detector. Changes due to the real part (f') and the imaginary part (f'') of the anomalous scattering can be measured and used separately, to find the heavy-atom position. Also, the real and imaginary components can be combined to improve Patterson and Fourier maps. The use of more accurate counter methods with the synchrotron source, such as a scintillation counter or preferably a multiwire proportional area detector should allow for accurate phase determination from diffraction data measured at three wavelengths.

We would like to acknowledge Dr J. Hastings for his assistance in the absolute-flux determination and other members of the Stanford Synchrotron Radiation Project staff for their technical assistance in support of this project. We thank Dr Brian Matthews for the permission to use his film scanner and Dr C. Sparks for suggesting the method of intensity measurement. This work was supported by grants from the National Cancer Institute (CA 16748) and the Research Corporation. KH is an Alfred P. Sloan Fellow, AW is recipient of the National Institutes of Health Research Service Award 1-F32-N505191, and JG is a NATO postdoctoral fellow.

APPENDIX
Polarization of synchrotron radiation

1. *Polarization factor for precession photographs made with polarized radiation*

The SPEAR synchrotron radiation source emits an X-ray beam which is almost totally polarized in the horizontal plane. Consequently, it is necessary to examine what form of the Lorentz–polarization factor should be applied to diffraction data collected from the SPEAR source. Waser (1951) has derived the expression for precession photographs made with unpolarized radiation. The geometry and notation of that paper will be used here. Whittaker (1953) has discussed the problem for inclined-beam photographs made with polarized radiation. Azaroff (1955) has derived expressions for the case of a partially polarized beam and for several types of diffraction methods, but the discussion for the precession method is incomplete. An expression for the Lorentz–polarization correction, which includes an absorption correction, has been derived (Burbank & Knox, 1962). Absorption errors are not considered in the present work.

The scattering of polarized X-rays by electrons. The scattered intensity is proportional to $\sin^2\varphi$, where φ is the angle between the direction of propagation of the scattered X-ray and the direction of polarization of the incident X-ray (see, for example, Buerger, 1960).

If the incident X-ray can be split up into two perpendicularly polarized components, the scattered amplitudes can be calculated separately with the above method. The total scattered intensity is then obtained from the sum of the squares of the two scattered amplitudes (Azaroff, 1955).

During the precession motion, the orientation of a particular reciprocal-lattice vector, relative to the incident X-ray beam, changes constantly. At two instances in one cycle of the motion, diffraction occurs from the corresponding Bragg planes. The instantaneous orientation of the reciprocal-lattice vector fixes the direction of the diffracted beam and hence φ for any given polarization of the incident beam.

The precession motion. The precession motion may be described with two systems of axes $\mathbf{i},\mathbf{j},\mathbf{k}$ being fixed with the camera and X-ray beam, $\mathbf{i}',\mathbf{j}',\mathbf{k}'$ being tied to the reciprocal lattice of the precessing crystal (see Fig. 1 of Waser, 1951). Because of the nature of the Z axis universal joint used in a precession camera, $\mathbf{k}'$ stays in the horizontal plane, α is the angle between $\mathbf{i}$ and $\mathbf{i}'$, β is the angle between $\mathbf{k}$ and $\mathbf{k}'$. The transform from the stationary to the moving frame is given by the equations:

$$\mathbf{i}' = \mathbf{i}\cos\alpha - \mathbf{j}\sin\alpha \tag{1}$$

$$\mathbf{j}' = \mathbf{i}\sin\alpha\cos\beta + \mathbf{j}\cos\alpha\cos\beta + \mathbf{k}\sin\beta \tag{2}$$

$$\mathbf{k}' = -\mathbf{i}\sin\alpha\sin\beta - \mathbf{j}\cos\alpha\sin\beta + \mathbf{k}\cos\beta \tag{3}$$

(Waser, 1951). The equations for the reverse transform are easily derived.

$$\mathbf{i} = \mathbf{i}'\cos\alpha + \mathbf{j}'\cos\beta\sin\alpha - \mathbf{k}'\sin\beta\sin\alpha \tag{4}$$

$$\mathbf{j} = -\mathbf{i}'\sin\alpha + \mathbf{j}'\cos\beta\cos\alpha - \mathbf{k}'\sin\beta\cos\alpha \tag{5}$$

$$\mathbf{k} = \mathbf{j}'\sin\beta + \mathbf{k}'\cos\beta. \tag{6}$$

Diffraction condition. The reciprocal-lattice point (x',y',z') intercepts the Ewald sphere when the center of the sphere is at the position:

$$x'_0 = \sin\mu\cos\tau_0, \quad y'_0 = -\cos\mu, \quad z'_0 = \sin\mu\sin\tau_0 \tag{7}$$

in the moving-coordinate system (Waser, 1951). μ is the precession angle. $\tau_0 = \tau + \eta$ or $\tau - \eta$ (*i.e.* the reciprocal-lattice point intercepts twice per revolution), where τ and η are the angles involved in the Lorentz factor and are defined by Waser (1951, Figs. 3 and 4). τ and η are calculable from the coordinates of the reciprocal-lattice point. In the stationary coordinate system the center of the Ewald sphere is

$$x_0 = 0, \quad y_0 = -1, \quad z_0 = 0. \tag{8}$$

Therefore, with the values of equations (7) and (8) used in equation (6) one finds that

$$0 = -\cos\mu\sin\beta + \sin\mu\sin\tau_0\cos\beta, \tag{9}$$

$$\textit{i.e.}\ \tan\beta = \tan\mu\sin\tau_0. \tag{10}$$

From equation (2) of Waser (1951),

$$\cos\alpha = \frac{\cos\mu}{\cos\beta}. \tag{11}$$

Equations (10) and (11) suffice to determine the magnitudes of α and β for a given reciprocal-lattice point and precession angle. The signs may be obtained from the following rules.

α positive if $-\pi/2 \le \tau_0 \le \pi/2$; if otherwise, α is negative.

β positive if $0 \le \tau_0 \le \pi$; if otherwise, β is negative.

Now the position of the diffraction spot when it intersects the Ewald sphere is obtained by transforming its coordinates in the reciprocal space tied to the crystal, to the coordinates fixed with the camera and X-ray beam with the above values of α and β; *i.e.*

$$x = x' \cos\alpha + y' \cos\beta \sin\alpha - z' \sin\beta \sin\alpha \quad (12)$$

$$y = -x' \sin\alpha + y' \cos\beta \cos\alpha - z' \sin\beta \cos\alpha \quad (13)$$

$$z = y' \sin\beta + z' \cos\beta. \quad (14)$$

The reciprocal-lattice vector at the instant of diffraction from the corresponding Bragg planes is thus

$$x\mathbf{i} + y\mathbf{j} + z\mathbf{k}. \quad (15)$$

To obtain the corresponding diffracted-beam vector one must add the incident-beam vector (**j**). The result is

$$x\mathbf{i} + (y+1)\mathbf{j} + z\mathbf{k}. \quad (16)$$

Note that the position of the diffraction spot in the coordinates fixed with the X-ray beam is not faithfully recorded by the film as the film is moving. Thus the direction of the diffracted ray, in real space, is not directly related to the position of the spot on the film.

The incident and diffracted beams are of the same wavelength. The length of the diffracted-beam vector, in reciprocal-lattice units, is therefore unity. The angles φ_x and φ_z between the diffracted beam and the **i** and **k** axes are given by

$$\cos\varphi_x = x, \quad \cos\varphi_z = z \quad (17)$$

and the polarization factor is given by

$$(1-x^2)f_h + (1-z^2)f_v \quad (18)$$

where f_h and f_v are the relative intensities in the horizontal and vertical directions.

This factor must be applied twice, once for each value of τ and must multiply the appropriate part of the Lorentz factor. The part which for unpolarized radiation is (Waser, 1951)

$$\tfrac{1}{2}(1+\cos^2 2\theta)\left[\frac{1}{1+\tan^2(\mu)\sin^2(\tau+\eta)} + \frac{1}{1+\tan^2(\mu)\sin^2(\tau-\eta)}\right] \quad (19)$$

becomes:

$$\frac{(1-x_+^2)f_h + (1-z_+^2)f_v}{1+\tan^2(\mu)\sin^2(\tau+\eta)} + \frac{(1-x_-^2)f_h + (1-z_-^2)f_v}{1+\tan^2(\mu)\sin^2(\tau-\eta)}, \quad (20)$$

x_+, z_+ being the x and z calculated for $\tau_0 = \tau + \eta$ and x_-, z_- being those calculated for $\tau_0 = \tau - \eta$.

Calculation of Lp factor for various polarizations. Lp factors, applicable to a series of precession photographs, were calculated on a computer with the above formula. There is a great difference between the values of the Lp factor for unpolarized and totally polarized radiation. For a 30° (*hk*0) precession photograph, in some regions of the film the Lp factors were in ratio 1·8:1. For smaller precession angles the disparity is reduced. For a 15° film, 1·15:1 is about the largest difference. There is only a 1% difference for a 5° (*hk*0) photograph over most of the film. On upper-level photographs, the differences are slightly larger for the same precession angle. For example, a 15° (*hk*2) film has Lp factors in ratio 1·2:1 in one region and for 5° (*hk*5) 1·15:1 is the largest ratio. For upper levels, a reciprocal-lattice spacing of 0·02 r.l.u. was used. There are substantial differences in the Lp factors for totally polarized and partially polarized beams also.

It is clear that the polarization of the incident X-rays must be taken into account if diffraction data collected using a synchrotron source and the precession method are to be used for structure determination.

2. *Determination of polarization of the synchrotron beam*

To test the degree of polarization of synchrotron radiation, calculations of the mean difference between symmetry-related reflections on each of the seven 25° precession photographs of the (*hk*0) plane of rubredoxin were made assuming various values of the polarization. Rubredoxin crystals are trigonal so there are three symmetry-related reflections on the (*hk*0) plane. They are 120° apart so the Lp factors are different in each case.

The value of the polarization which gave the smallest mean difference between symmetry-related reflections for a given film was taken to be correct for that film. For the seven rubredoxin films the values for the polarization varied from 63 to 85% (of intensity in the horizontal direction), indicating that the method is not very precise. More accurate measurements will be necessary in the future.

References

ARGOS, P. & MATHEWS, F. S. (1973). *Acta Cryst.* B**29**, 1604–1611.

AZAROFF, L. V. (1955). *Acta Cryst.* **8**, 701–704.

BARRINGTON LEIGH, J., HOLMES, K. C. & ROSENBAUM, G. (1972). In *Research Applications of Synchrotron Radiation*, Publication BNL 50381, Brookhaven National Laboratory, USA.

BARRINGTON LEIGH, J. & ROSENBAUM, G. (1974). *J. Appl. Cryst.* **7**, 117–121.

BLAKE, C. C. F. & EVANS, P. R. (1974). *J. Mol. Biol.* **84**, 585–601.

BLOW, D. M. (1958). *Proc. Roy. Soc.* A**247**, 302–336.

BLOW, D. M. & ROSSMANN, M. G. (1961). *Acta Cryst.* **14**, 1195–1202.

BORDAS, J., MUNRO, I. H. & GLAZER, A. M. (1976). *Nature, Lond.* **262**, 541–545.

BUERGER, M. J. (1960). *Crystal Structure Analysis*, p. 25. New York: John Wiley.

BURBANK, R. D. & KNOX, K. (1962). *Rev. Sci. Instrum.* **33**, 218–222.

COLMAN, P. M., JANSONIUS, J. N. & MATTHEWS, B. W. (1972). *J. Mol. Biol.* **70**, 701–724.

FUKAMACHI, T. & HOSOYA, S. (1975). *Acta Cryst.* A**31**, 215–220.
GOODY, R. S., HOLMES, K. C., MANNHERZ, H. G., BARRINGTON LEIGH, J. & ROSENBAUM, G. (1975). *Biophys. J.* **15**, 687–705.
HARMSEN, A., LEBERMAN, R. & SCHULZ, G. E. (1976). *J. Mol. Biol.* **104**, 311–314.
HASELGROVE, J. C. (1976). Private communication.
HERRIOTT, J. R., SIEKER, L. C., JENSEN, L. H. & LOVENBERG, W. (1970). *J. Mol. Biol.* **50**, 391–406.
HERZENBERG, A. & LAU, H. S. M. (1967). *Acta Cryst.* **22**, 24–28.
HOPPE, W. & JAKUBOWSKI, U. (1975). *Anomalous Scattering*, edited by S. RAMASESHAN & S. C. ABRAHAMS, pp. 437–461. Copenhagen: Munksgaard.
KARTHA, G. & PARTHASARATHY, R. (1965). *Acta Cryst.* **18**, 745–749.
KNOX, J. R., KELLY, J. A., MOEWS, P. C. & MURTHY, N. S. (1976). *J. Mol. Biol.* **104**, 865–875.
KRAUT, J., HIGH, D. F. & SIEKER, L. C. (1964). *Proc. Natl. Acad. Sci. USA*, **51**, 839–845.
MATTHEWS, B. W. (1966). *Acta Cryst.* **20**, 230–239.
MATTHEWS, B. W., KLOPFENSTEIN, C. E. & COLMAN, P. M. (1972). *J. Phys. E: Sci. Instrum.* **5**, 353–359.
MOKULSKAYA, T. D., MOKULSKII, M. A., NIKITIN, A. A., ANASHIN, V. V., KUPLIPANOV, G. N., LUKASHEV, V. A. & SKRINSKII, A. N. (1974). *Akad. Nauk. SSSR Dokl.* **218**, 824–827.
PATTERSON, A. L. & LOVE, W. E. (1960). *Amer. Min.* **45**, 325–333.
PHILLIPS, J. C., WLODAWER, A., YEVITZ, M. M. & HODGSON, K. O. (1976). *Proc. Natl. Acad. Sci. USA*, **73**, 128–132.
RAMAN, S. (1959). *Proc. Ind. Acad. Sci.* **50A**, 95–107.
RAMASESHAN, S. (1964). In *Advanced Methods in Crystallography*, edited by G. N. RAMACHANDRAN, London: Academic Press.
RAMASESHAN, S. & ABRAHAMS, S. C. (1975). *Anomalous Scattering*. Copenhagen: Munksgaard.
ROSENBAUM, G., HOLMES, K. C. & WITZ, J. (1971). *Nature, Lond.* **230**, 434–437.
SCHOENBORN, B. P. (1975). *Anomalous Scattering*, edited by S. RAMASESHAN & S. C. ABRAHAMS, pp. 407–416. Copenhagen: Munksgaard.
SIEKER, L. C., ADMAN, E. & JENSEN, L. H. (1972). *Nature, Lond.* **235**, 40–42.
SINGH, A. K. & RAMASESHAN, S. (1968). *Acta Cryst.* B**24**, 35–39.
SPARKS, C. J. (1976). *Advances in X-ray Analysis*, edited by R. W. GOULD, C. S. BARRETT, J. B. NEWKIRK & C. O. RUUD, Vol. 19, pp. 19–52. Dubuque, Iowa: Kendall/Hunt.
STENKAMP, R. E., SIEKER, L. C., JENSEN, L. H. & LOEHR, J. S. (1976). *J. Mol. Biol.* **100**, 23–34.
Synchrotron Radiation Research (1976). Edited by K. O. HODGSON, H. WINICK & G. CHU, Stanford Synchrotron Radiation Project, Stanford, California, USA.
WASER, J. (1951). *Rev. Sci. Instrum.* **22**, 563–566.
WATENPAUGH, K. D., SIEKER, L. C., HERRIOTT, J. R. & JENSEN, L. H. (1973). *Acta Cryst.* B**29**, 943–956.
WATENPAUGH, K. D., SIEKER, L. C., JENSEN, L. H., LEGALL, J. & DUBOURDIEU, M. (1972). *Proc. Natl. Acad. Sci. USA*, **69**, 3185–3188.
WEBB, N. G. (1976). *Rev. Sci. Instrum.* **47**, 545–547.
WEBB, N. G., SAMSON, S., STROUD, R. M., GAMBLE, R. C. & BALDESCHWIELER, J. D. (1976). *Rev. Sci. Instrum.* **47**, 836–839.
WEBB, N. G., SAMSON, S., STROUD, R. M., GAMBLE, R. C. & BALDESCHWIELER, J. D. (1977). *J. Appl. Cryst.* **10**, 104–110.
WHITTAKER, E. J. W. (1953). *Acta Cryst.* **6**, 222–223.
WINICK, H. (1974). *Proc. 9th Internat. Conf. High Energy Accelerators*, pp. 685–688. Stanford Linear Accelerator Center, Stanford, California.